LIMNOLOGY
and
OCEANOGRAPHY

ASLO

Limnol. Oceanogr. 9999, 2020, 1–17

doi: 10.1002/lno.11623

Thin layers in the coastal zone of Ubatuba, Brazil: Mechanisms of formation and dissipation

Silvana B. Penninck,[1,2] **Rubens M. Lopes**,[1,*] **Josiane F. Lima**,[1] **Margaret A. McManus**[2]
[1]Department of Biological Oceanography, Oceanographic Institute, University of São Paulo, SP, Brazil
[2]Department of Oceanography, University of Hawai'i at Mānoa, Honolulu, Hawaii

Abstract

Thin layers are vertically compressed, horizontally extensive, highly concentrated features comprised of plankton and/or particles. They are critical components of the marine ecosystem, likely playing a key role in the life histories and evolutionary trajectories of species found in, or, interacting with them. These structures have been reported in diverse marine environments around the globe. However, the mechanisms of thin layer formation/dissipation in the southwestern Atlantic Ocean were unknown until this contribution. To assess the temporal evolution of thin phytoplankton layers on the inner shelf off Ubatuba, Brazil, we conducted two oceanographic fixed station cruises, including optics, acoustics, and imaging techniques. Over a period of 2 days, three thin layers were observed: within the pycnocline close to the maximum stratification, and below the pycnocline where phytoplankton were affected by enhanced nutrient supply provided by the South Atlantic Central Water (SACW). Changes in regional wind patterns influenced the presence of SACW, which directly affected shear and stratification: the primary physical mechanisms we attribute to thin layer formation in this region. The associated biological mechanisms contributing to thin layer formation were biomass accumulation (in situ growth) and likely the mobility of dinoflagellates. The dominant organisms in the thin layer depths and surroundings, by our in situ imaging system, were cyanobacteria, diatoms, dinoflagellates, and crustaceans. Thin Layers likely have crucial importance for meso-oligotrophic environments, representing important feeding resources for higher trophic levels.

The vertical distribution of plankton is influenced by an interplay of physical, chemical and biological factors that can lead to the formation of structures called "thin layers." Thin layers are features with accumulation of plankton or particles on a vertical scale from centimeters to a few meters (Donaghay et al. 1992), often extending horizontally for kilometers (Cowles et al. 1998) and persisting for hours to several days. Fine-scale aggregations of phytoplankton are common features and can be found in a wide variety of environments, being recurrent in stratified coastal and ocean waters (Sullivan et al. 2010).

Marine phytoplankton influence the abundance and diversity of organisms, stimulate the functioning of the marine ecosystem and determine the maximum limits for fishery production (Chassot et al. 2010), in addition to exerting a strong influence on climatic processes and biogeochemical cycles (Roemmich and McGowan 1995). Previous research has pointed out important implications of thin layers of phytoplankton for trophic dynamics (Benoit-Bird et al. 2009), carbon fluxes in the ocean (Bochdansky et al. 2010) and harmful algal blooms (McManus et al. 2008). Thin layers represent an important food resource that is restricted vertically in the water column and important in determining the nutrition and survival of grazers (Mullin and Brooks 1976). The presence of thin layers likely alters local concentrations of nutrients, toxins and organisms, playing an important role in biological processes in coastal environments (Cowles et al. 1998).

In view of their role in planktonic ecosystems, it is essential to determine what controls the formation of thin plankton layers. Thin layers can be generated by a variety of biological and physical mechanisms, including cell behavior, morphology, population dynamics, fluid stratification and vertical current shear (Durham and Stocker 2012). Studies have documented the processes involved in the formation and persistence of thin layers in coastal regions (McManus et al. 2012; Barnett et al. 2019) and in frontal and coastal upwelling zones (De Verneil et al. 2019).

*Correspondence: rubens@usp.br

Additional Supporting Information may be found in the online version of this article.

Dekshenieks et al. (2001) presented one of the first quantitative studies of thin layers and the associated physical processes, in a Northern Pacific fjord, and emphasized the importance of studying local circulation patterns and regional physical forcing in understanding the dynamics of these features. Cheriton et al. (2007) studied the occurrence of thin layers along the west coast of the U.S., noting that a change in regional wind patterns precipitated a change in physical structure of the water column, leading to the absence of thin layers of zooplankton. Stacey et al. (2007) point out that the turbulent diffusion caused by regional winds, convective processes and action of internal waves act as divergent or dissipating processes of layers, while the vertical current shear, the passive deposition of phytoplankton on a density surface and the phytoplankton mobility act as convergent, layer-forming processes.

Thin layers are often related to the pycnocline, thermocline or halocline (Dekshenieks et al. 2001; Steinbuck et al. 2009; Breckenridge and Bollens 2010) and have been reported in environments with both low shear and turbulent mixing. Shroyer et al. (2014) identified thin biological layers in regions where intense mixing events were rare, within the pycnocline (close to maximum stratification) and at the base of the pycnocline. Talapatra et al. (2013) found several peaks of *Chaetoceros socialis* colonies, nonmotile diatoms, near the pycnocline, in a region of almost zero shear, low rates of dissipation and high stratification. Onitsuka et al. (2018) observed the temporal evolution of a diatom-rich layer formed just below the pycnocline, where the turbulent mixture was weak, in a stratified bay in Japan.

Studies on fine-scale plankton structures have been highly dependent on available technology and sampling methodologies (McManus et al. 2012). Effective measurement methods comprise profiling with high vertical resolution (order of centimeters), typically from sensors with slow deployment speeds through the water column and/or high sampling rates. In addition, the decrease in the effects of the vessel's movement during profiling must be considered, using free-fall sensors or from platforms decoupled from the vessel (Sullivan et al. 2010).

In this study, optical and acoustic sensors and a high resolution imaging system were combined to investigate the occurrence, persistence and dissipation of fine-scale phytoplankton aggregations and to study the influence of these structures on zooplankton distributions. Thin layers of phytoplankton were observed in the coastal waters of Ubatuba, southeastern Brazil, in February 2019 during the summer, when vertical stratification associated with bottom intrusions of cold and nutrient-rich water occur.

Motivated by the hypothesis that physical constraints provide an appropriate environment for the formation of thin layers in the study area, and that their presence has important ecological implications to this meso-oligotrophic environment, this work investigates the short-term temporal changes in phytoplankton vertical distribution and its relationship with physical and biological processes, and represents the first study on thin layers in the southwestern Atlantic Ocean.

Study site

The study area is in the central part of the Southeastern Brazilian Continental Shelf (SBCS), on the inner shelf off Ubatuba, on the north coast of São Paulo, Brazil (Fig. 1a). Due to the South Atlantic Subtropical Anticyclone, in the summer months (i.e., December to March), winds are predominantly from the northeast on the Brazilian continental shelf between 20°S and 30°S. In the winter months (i.e., June to September), the winds are predominantly from the south and southwest associated with the passage of cold fronts (Reboita et al. 2019). The inner shelf circulation dynamics are controlled by the winds, while the outer shelf circulation dynamics are influenced by the Brazil Current (Castro and Lee 1995).

The tidal currents on the continental shelf are low in energy and no large river discharges exist. Hydrodynamic energy in this region is considered low to moderate, due to the presence of islands (Ilhabela, Mar Virado and Anchieta Islands), which act as a barrier to the action of waves from the open ocean (Batista and Harari 2017). These are the reasons why winds have been identified as the primary forcing mechanism of circulation on the SBCS (Mazzini 2009).

The shelf region off Ubatuba is influenced by the following water bodies: Tropical Water (TW; relatively high salinity, high temperature, low nutrient concentration), Coastal Water (CW; relatively low salinity, high temperature, variable nutrient concentration) and South Atlantic Central Water (SACW; relatively low temperature, high nutrient concentration). Predominant winds from the E-NE quadrant induced SACW penetration onto the shelf by Ekman transport from late spring to late summer (Castro Filho et al. 1987). The coastal water in the surface moves offshore (Ekman transport is to the left of the wind in the southern hemisphere), inducing the SACW to intrude toward the coast near the bottom, sometimes reaching the euphotic zone (Miranda and Katsuragawa 1991). When SACW intrudes onshore from the slope onto the inner shelf, a strong stratification is established at midwater depth. Despite the nutrient enrichment during the summer caused by the SACW, previous studies in the region point to meso-oligotrophic conditions prevalent near the surface for most of the year, due to relatively low nutrient levels (Sassi and Kutner 1982; Aidar et al. 1993).

Materials and methods

Sampling—fixed stations

A fixed oceanographic station was occupied in two consecutive 12-h intervals from 8:00 h to 20:00 h on February 20 and 21, 2019, aboard the 14 m research boat *Veliger II* of the Oceanographic Institute of the University of São Paulo (IOUSP), at the study site (Fig. 1b; 45°5.533′ W, 23°35.318′ S).

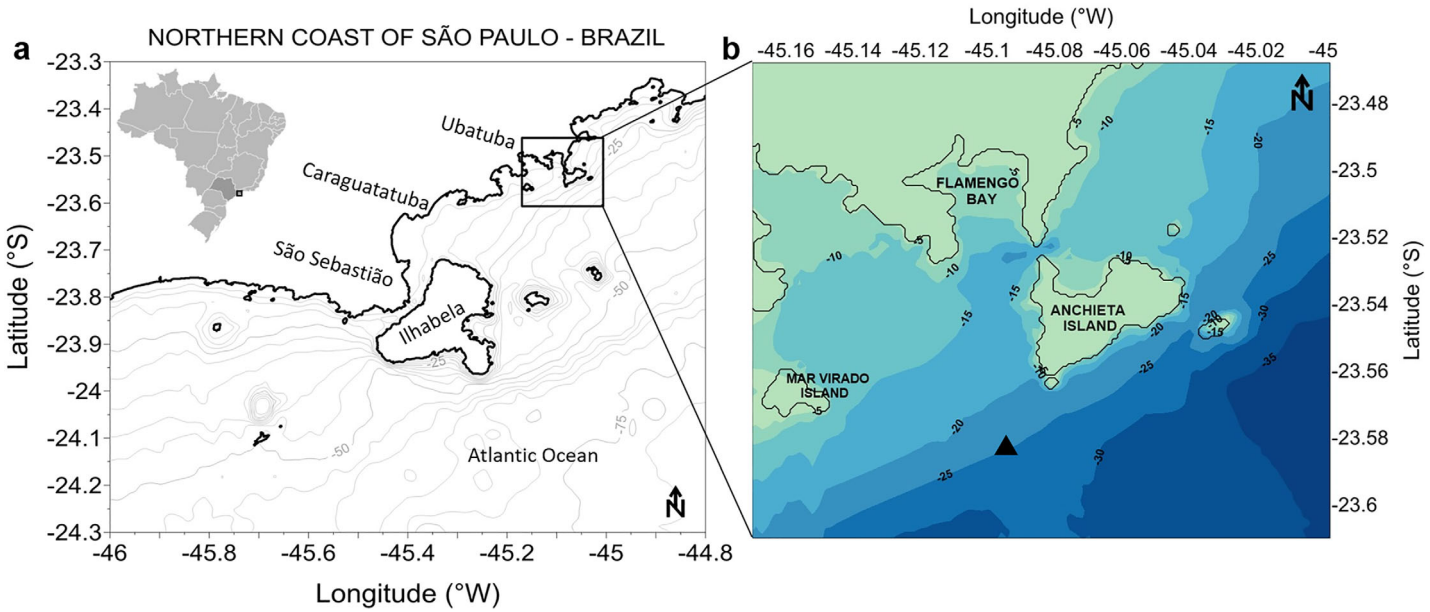

Fig 1. (**a**) Map of the northern coast of the state of São Paulo, Brazil, with a high-resolution view of the Southeastern Brazilian Continental Shelf (SBCS) located on the inner shelf off Ubatuba. (**b**) High resolution view of the study area. The location of the fixed-point sampling station is indicated by the closed black triangle (25 m isobath). Bathymetric contours are in increments of 5 m, where dark blue represents deeper depths.

During these intervals, profiles were collected roughly every 30-min, resulting in a total of 48 profiles over 2 days. The RINKO-profiler and a plankton imaging system and were attached to the same frame for simultaneous profiling. The sinking speed (~ 0.27 m s^{-1}) and buoyancy of the instrumentation packaged were controlled by adding floats to the frame to reduce turbulence during lowering.

A high resolution multiparameter RINKO-profiler (JFE Advantech) was used to obtain fine-scale profiles of water temperature, salinity, chlorophyll *a* fluorescence (Chl-Flu) and turbidity (optical backscatter intensity) at 0.1 m intervals (depth trigger mode) at each station (Fig. 2b). Table 1 presents the specifications of the sensors used.

A plankton imaging system was used to obtain qualitative and quantitative plankton data (Fig. 2a). The system, based on shadowgraphic imaging, is a prototype developed by IOUSP (Medeiros 2017), consisting of a collimated infrared LED beam and a high-resolution camera (4MP) with a frame rate ranging between 6 and 15 frames per second, pixel size of 5.5 μm and a volume of 4.5×10^{-6} m^3 per image. Computer vision processing tools developed at the Laboratory of Plankton Systems (LAPS-IOUSP) allowed for the characterization and classification of organisms down to taxonomic groups, using the Random Forest algorithm. The system captures particles above 5.5 μm, but only particles above 100 μm can be reliably identified in the taxonomic classification step.

For analysis of the chlorophyll *a* (Chl *a*) and nutrient concentrations, water was collected with a go-flo bottle every 4 h at various depth levels along the water column: surface (0 m), mixing layer (~ 5 m), top of the thermocline (~ 10 m), vicinity of the fluorescence peaks (~ 15 to ~ 21 m, at 2 m intervals) and bottom (~ 23 m). The water samples were filtered through a 25 mm GF/F filter immediately after collection and the filters were stored in an ultrafreezer (– 80°C) until the extraction of

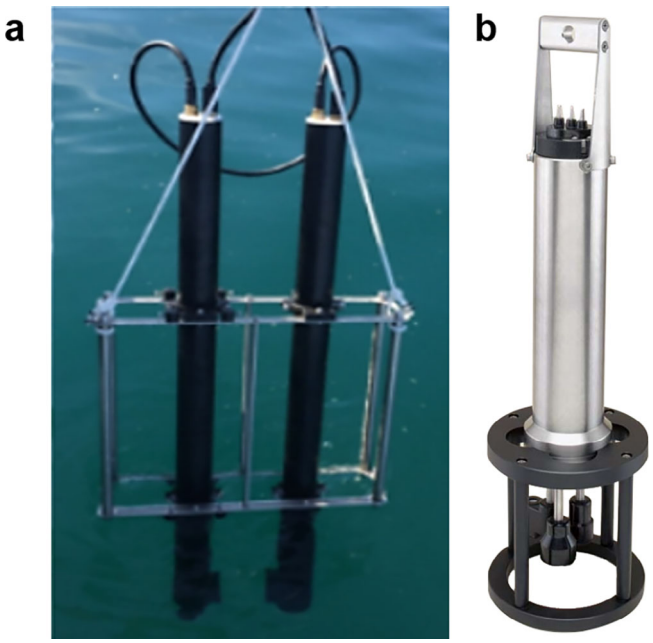

Fig 2. (**a**) Shadowgraphic imaging system consisting of two cylindrical pressure cases, both 1.12 m long and 9.5 cm wide. (**b**) Rinko-profiler, 49.1 cm long and 13.6 cm wide. The RINKO-profiler was coupled in the imaging system frame for simultaneous profiling.

Table 1. RINKO-profiler sensor specifications.

Sensor	Type	Resolution	Accuracy
Depth	Pressure sensor	0.01 m	±0.3% FS
Temperature	Thermistor	0.001°C	±0.01°C (0–35°C)
Salinity	Practical salinity	0.001	—
Turbidity	Backscattered light	0.03 FTU	±0.3 FTU or ±2% of measured value
Chlorophyll	Fluorometric	0.01 ppb	±1% FS (0–200 ppb)

Chl-*a* in the laboratory. Aliquots of the filtered water were separated and frozen (– 20°C) for analysis of dissolved inorganic nutrients (nitrite, nitrate, phosphate, and silicate). The nutrients were determined in the laboratory using a flow injection auto-analyzer. Chl-*a* concentrations were measured using a fluorometer (10-AU, Turner Designs) according to the method proposed by Welschmeyer (1994). The correlation coefficient between the Chl-Flu and the extracted Chl-*a* concentration was 0.89 (n = 50).

To obtain velocity data throughout the water column, a vessel-mounted downward-looking Sontek 500-kHz ADCP was used. The vessel-mounted ADCP made measurements from near-surface (~ 3 m) to near-bottom with 1.0 m vertical resolution, during the 12-h observations, on both days. The tidal level was predicted by harmonic analysis (Harari and Mesquita 2003). The hourly sea level data were provided by the Copernicus Marine Environment Monitoring Service (CMEMS). Wind data were obtained from the Climate Forecast System Version 2 (CFSv2), produced by the NOAA National Centers for Environmental Prediction (NCEP).

Calculation of physical variables

Stratification in the water column was estimated by calculating the Brunt-Väisälä Frequency (N^2). This parameter is related to both the stability of the water column and the vertical density gradient, and was calculated from:

$$N^2 = -\frac{g}{\rho_0}\left(\frac{\partial \rho}{\partial z}\right) \quad (1)$$

where g is the acceleration of gravity, z is the depth, ρ is the seawater density and ρ_0 is the average density (Pond and Pickard 1983). High N^2 values indicate a stratified portion of the water column, while low values are found in vertically homogeneous regions. The quantification of vertical shear (S^2) was determined by:

$$S^2 = \left(\frac{\partial U}{\partial z}\right)^2 + \left(\frac{\partial V}{\partial z}\right)^2 \quad (2)$$

where U and V are, respectively, the zonal and meridional components of the currents (Itsweire et al. 1989).

The Richardson number (Ri) defines the relative importance of stabilization due to vertical density stratification vs. destabilization due to vertical velocity shear, and was calculated by the following equation:

$$Ri = \frac{N^2}{S^2} \quad (3)$$

To analyze the effects of the wind forcing in the surface, a simplification of the Ekman transport (U_e), east-southeastward, considering the shoreline orientation, was estimated as:

$$U_e = \frac{\tau_y}{\rho_0 f} \quad (4)$$

where τ_y is the wind stress on the sea surface, obtained using the bulk formula (Stewart 2008), ρ_0 is the density of sea water (ρ_0 = 1025 kg/m^3), and f is the Coriolis parameter.

Estimation of the mean volume backscatter strength

The Sontek 500 kHz ADCP was initially deployed to measure water velocity, however it was also used to estimate the volume backscattering strength from the ADCP signal strength data (echo level). To estimate the volume backscattering strength, a rearrangement of the sonar equation was used (Sontek-YSI 1997; Deines 1999):

$$MVBS = C + 10\log_{10}\left[(T_x + 273.16)R^2\right] - L_{DBM} - P_{DBM} + 2\alpha R + K_c(E - E_r) \quad (5)$$

where C is a constant factor specific to the instrument used (dB); $MVBS$ is the mean volume backscattering strength (dB); T_x is the temperature detected at the transducer (°C); R is the slant rage (m); L_{DBM} is the $10\log_{10}$ of the transmit pulse length (1 m); P_{DBM} is the $10\log_{10}$ of the transmit power, specific for the instrument; α is the frequency-specific absorption coefficient in seawater (0.14 dB/m at 500 kHz); K_c is an instrument-specific constant that converts counts in decibels (in this case K_c = 0.43; Sontek-YSI 1997); E is echo level or signal strength (counts); and E_r is the noise level. Because C and P_{DBM} could not be accurately measured during sampling, they were set to zero. These missing parameters do not affect the objectives of the application of the acoustic data in this study. However, in this contribution the MVBS was considered an indirect and qualitative

proxy for relative zooplanktonic biomass, representing relative volume backscatter strength (RVBS).

Thin layer identification

During the evolution of research on thin layers the criteria for their identification have been customized for different environments. There is no standard for thin layer characterization in the literature, but there are some criteria to be followed for identification, which vary depending on the instruments to be used, type of organisms in the layer and region of study in the ocean (Dekshenieks et al. 2001; Sullivan et al. 2010).

For this work, three specific criteria were established to define a thin layer structure. (1) The fluorescence peak must be present in two or more subsequent profiles; this helps eliminate ephemeral structures. (2) The layer must be ≤ 3.61 m thick at half maximum intensity; this value was chosen based on previous studies (Dekshenieks et al. 2001; Ryan et al. 2008; McManus et al. 2012). (3) The intensity of the fluorescence peak must be at least 1.3 times the background levels, a signal intensity previously considered for oligotrophic or mesotrophic waters with low plankton biomass (Benoit-Bird et al. 2010; McManus et al. 2012).

Results

Meteorological and oceanographic conditions

On February 20th, 2019, winds were predominantly from the northwest and from the northeast with speeds from 3.60 to 5.70 m s^{-1} and 2.10 to 3.60 m s^{-1}, respectively (Fig. 3d). On February 21st, winds were predominantly from the southwest and southeast at speeds between 2.10 and 3.60 m s^{-1}, and from the east with speeds between 3.60 and 5.70 m s^{-1} (Fig. 3e). The wind fields for February 20th and 21st are illustrated in Fig. 3a. The ocean currents in this region have a predominant flow to the southwest; however, when cold fronts pass through the area from the southwest, the current direction is known to reverse and flow to the northeast (Castro et al. 2006). There were no cold fronts during our study.

The general shoreline orientation of the southeastern Brazilian coast, approximately southwest-northeast, and the shallow shelf with isobaths parallel to the coast, provides conditions for raising or lowering sea level by Ekman transport, due to the action of winds along the coast from southwest or northeast, respectively. Over the study days, there was an increase in sea surface height (Fig. 3b, solid line), of about + 0.1 m, while the Ekman transport (Fig. 3b, dashed line) changed direction from offshore (to east, positive signal) to onshore (to west, negative signal). This was most likely due to the relaxation of the winds from north-northeast (weak winds < 3 m s^{-1}) and an increase in winds from southwest-southeast.

The study took place during a spring tide. The tides in this region are semidiurnal with diurnal inequality (Mesquita and Harari 1983). On February 20th, the tide flooded from 09:49 h to 14:32 h, with a range of 0.80 m, and ebbed from 14:32 h to 22:13 h, with a range of 1.20 m. On February 21st, the tide flooded from 10:24 h to 15:00 h, with a range of 0.90 m and ebbed from 15:00 h to 23:00 h, again with a range of 1.20 m (Fig. 3c).

On February 20th, during the flood tide the currents flowed to east/northeast in subsurface (3–5 m) and, predominantly, to west between 7 and 18 m, and to northwest near the bottom, between 19 and 25 m (Fig. 4a1). During the ebb tide, the current direction was reversed to east/southeast (Fig. 4a2). On February 21st, during the flood tide, currents flowed to the east/northeast between the surface (3 m) and 15 m depth, while from 16 m to the bottom the currents underwent anticyclonic rotation, flowing to the west/northwest (Fig. 4b1). On ebb tide, the predominant flow throughout the water column was to the east, except for a rotation in current to the north between 18 and 21 m (Fig. 4b2).

Thin layer observations

Three thin layers were observed on February 20th (Fig. 5a). In the 24 profiles on February 20th, 50 fluorometric chlorophyll (Chl-Flu) peaks were detected, among which 45 (90%) were considered discrete observations of the 3 thin layers. Sixty percent of these observations were within the pycnocline, while 40% were below the pycnocline. The average Chl-Flu intensity in the thin layer depths inside the pycnocline was 2.12 μg L^{-1}, and the thickness averaged 0.85 m. The Chl-Flu intensity in the layer depths below the pycnocline averaged 3.62 μg L^{-1}, and the thickness averaged 2.27 m.

The vertical distribution of Chl *a* fluorescence and density indicated that thin layers closely followed the 25.4, the 23.75 and the 24.5 isopycnals (Fig. 5a). The TS-Chl-Flu diagram confirmed the presence of SACW ($T < 20$°C and $S < 36.40$; Miranda and Katsuragawa 1991) associated with higher Chl-Flu intensity (Fig. 5c). The water column was strongly stratified, with temperatures that ranged from 29°C in the surface and 18.6°C near the bottom, and salinities that varied from 34.0, in the surface, to 36.5, near the bottom. The average concentrations of dissolved nutrients at the surface were: 0.08 μM for nitrite, 0.60 μM for nitrate, 0.18 μM for phosphate and 5.44 μM for silicate. Near the bottom, the average nutrient concentrations were: 0.93 μM for nitrite, 3.16 μM for nitrate, 0.64 μM for phosphate and 10.00 μM for silicate. These high concentrations of nutrients in the bottom corroborate the presence of SACW in this zone.

The overall vertical distribution of particles (Fig. 6) captured by the imaging system reveals higher particle concentration at the surface (0–5 m; ~ 200×10^3 Particles L^{-1}), near the thin layers (13–16 m, ~ 10×10^3 Particles L^{-1}; and 19–21 m, ~ 50×10^3 Particles L^{-1}), and a particle aggregation near the bottom (> 23 m, ~ 170×10^3 Particles L^{-1}), presumably because of bottom sediment resuspension (after Ryan et al. 2014) caused by the increase in the current shear close to the bottom (Fig. 5e). Full-frame images provided an overall assessment of particle occurrence in different layers (Fig. 6a1–d1). The water

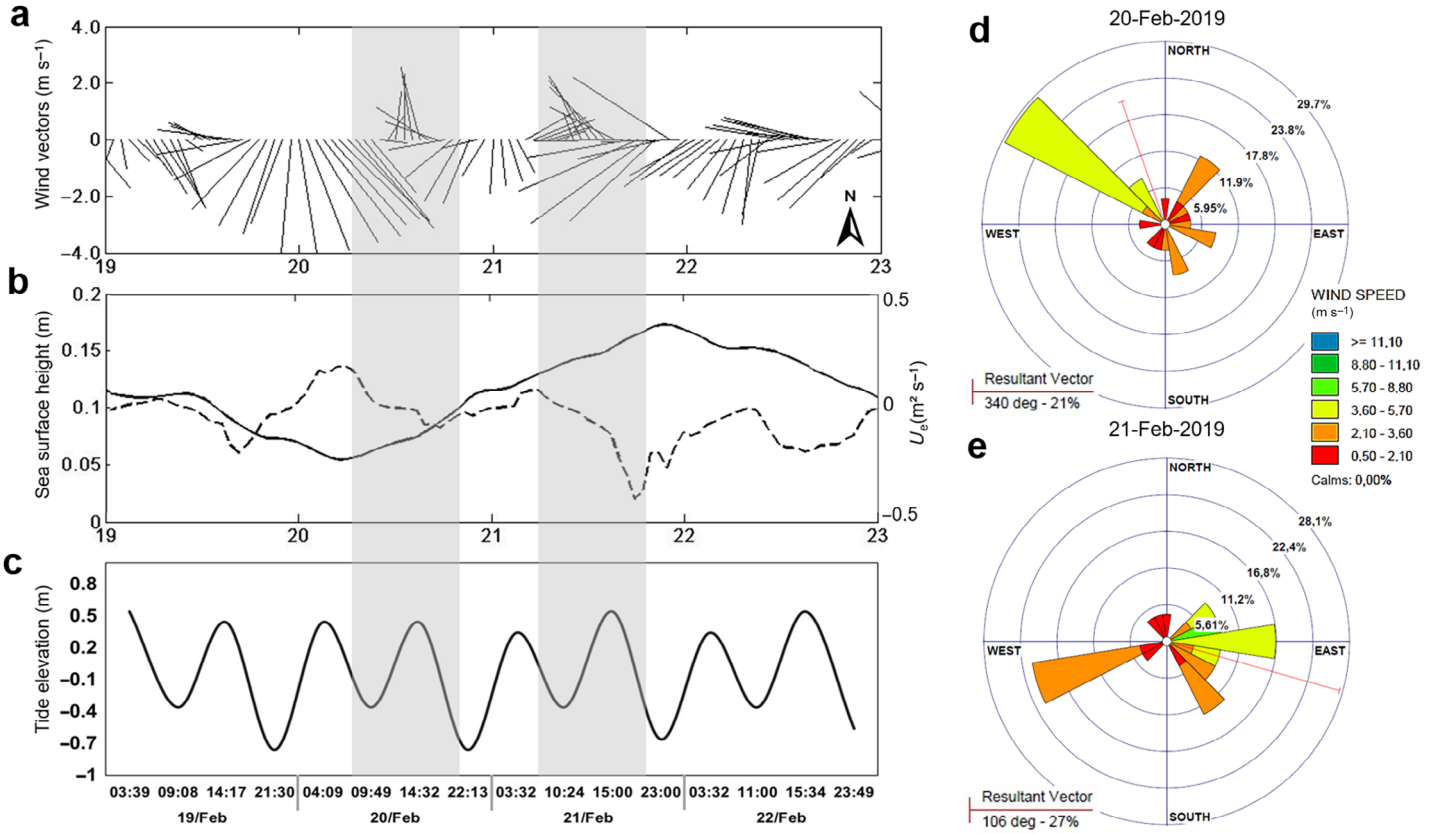

Fig 3. Wind and ocean conditions between Feb 19 and 23, 2019. (**a**) Stick plots showing the direction the wind is "going to" and magnitude of the wind speed (data from CFSv2/NCEP). (**b**) Sea surface height (m; left axis) (solid line) (provided by CMEMS). Ekman transport, *Ue* (m^2 s^{-1}; right axis), in the surface layer (dashed line). (**c**) Predicted tidal curve (m) with the times of occurrence of high and low tide levels. The shadows display the fixed-stations periods on Feb 20th and 21st. (**d**) Wind rose for Feb 20th, (**e**) wind rose for Feb 21st. Wind rose (direction frequency) indicates the direction the wind is coming from. The red lines in (d) and (e) are the resultant vector derived from the wind direction data. Wind speed range is indicated on the color bar (red: 0.50–-2.10 m s^{-1}; orange: 2.10–3.60 m s^{-1}; yellow: 3.60–5.70 m s^{-1}; light green: 5.70–8.80 m s^{-1}; dark green: 8.80–11.10 m s^{-1}; blue: ≥ 11.10 m s^{-1}).

in the layer regions ~ 20 m (Fig. 6c1) and near the bottom (Fig. 6d1) visually appeared to be more turbid. The shadowgraphic system captured small disturbances in a thin fluid layer on the top of the pycnocline (~ 15 m) with a "mixing appearance" seen in the images in Fig. 6b1. This appearance is likely due to small turbulence induced by diffusive convection in the presence of small density inversions. According to Yoshida et al. (1987), even with very small density differences between fluids double diffusive effects can produce inhomogeneity of density and induce currents (shear).

A video recorded by the imaging system during vertical profiling was provided for the online version of this publication (Supporting Information Video S1). In the video, it is possible to observe when the instrumentation passes through the region with fluid disturbances on the top of the pycnocline (similar to Fig. 6b1), and through the thin layers as it drops to the bottom.

The classification results for February 20th showed mesozooplankton (appendicularians, cnidarians, chaetognaths, cladocerans and copepods) peaks between 0 and 5 m (Fig. 6a2). There were higher concentrations of appendicularians (~ 50 Ind L^{-1}) and cnidarians (~ 20 Ind L^{-1}) near the surface (0–3 m) and in the mixed layer (~ 5 and 9–10 m), respectively, while the concentrations of crustaceans were higher between 15 and 24 m, reaching a maximum of ~ 80 Ind L^{-1} (Fig. 7a).

In the region between 18 and 22 m cyanobacteria and diatoms were observed most frequently. The regions above and below the pycnocline (~ 15 and ~ 20 m, respectively) showed corresponding turbidity (optical backscattering) and Chl-Flu peaks (Fig. 7a). Within the pycnocline diatoms, dinoflagellates and cyanobacteria were identified (Fig. 6b2). Below the pycnocline there was a noticeable increase in cyanobacterial concentration (~ 80 Ind L^{-1}), but many diatom species were also identified in the thin layer region (Fig. 6c2).

On February 21st, there was an enhancement in the cyanobacterial population between 11 and 20 m depth compared to the previous day, reaching a maximum of ~ 150 Ind L^{-1}. This

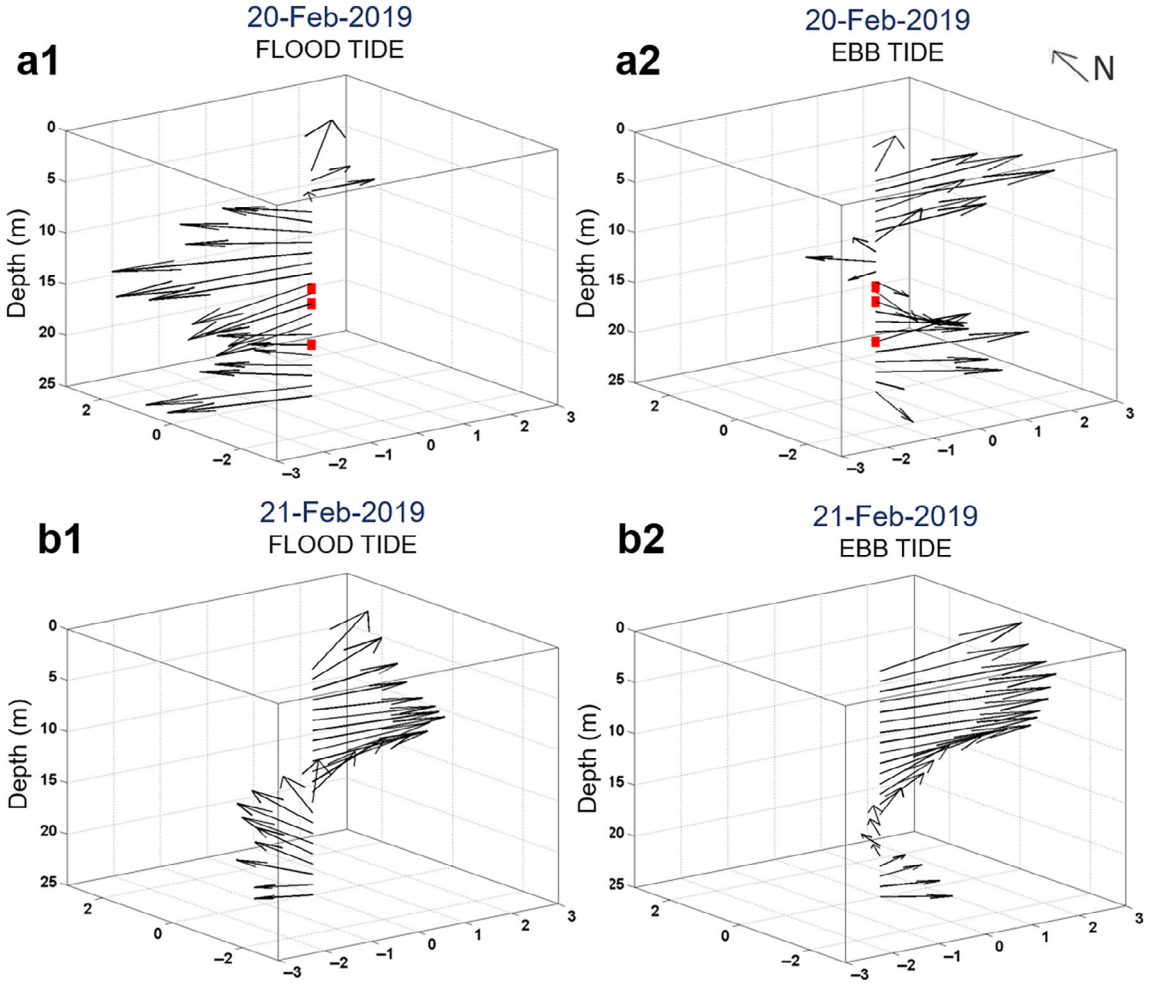

Fig 4. (**a**) ADCP measured currents (m s^{-1}) from near-surface to near bottom on Feb 20th. (**a1**) Average of the current vectors during the flood tide; (**a2**) average of the current vectors during the ebb tide. The red markings indicate the medium depths where thin layers were observed (at ~ 14.5, ~ 16, and ~ 20 m). (**b**) ADCP measured currents (m s^{-1}) from near-surface to near bottom on Feb 21st. (**b1**) Average of the current vectors during the flood tide; (**b2**) average of current vectors during the ebb tide.

enhancement was accompanied by an increase in crustacean concentration and in Chl-Flu and turbidity signals (Fig. 7b).

The RVBS (in dB), obtained from ADCP acoustic backscatter data, is a measure that can be used to estimate the relative amount of particles suspended in the water (such as sediments, organisms or bubbles) (Guerra et al. 2019). On February 20th, the RVBS distribution revealed higher values (> 65 dB) in the upper mixed layer (~ 3–6 m) and near-bottom (24–25 m; Fig. 7c). This result shows relationships to the particle concentration profile obtained by the imaging system (Fig. 7d), indicating a peak of particles in the surface and another peak in the bottom.

Thin layer formation

Thin layers within the pycnocline were associated with median values of $N^2 = 0.89 \times 10^{-4}$ s^{-2} and $S^2 = 0.37 \times 10^{-4}$ s^{-2}. The thin layers below the pycnocline were associated with lower stratification, $N^2 = 0.12 \times 10^{-4}$ s^{-2} (median value), and with higher current shear, $S^2 = 0.89 \times 10^{-4}$ s^{-2} (Table 2). The Richardson number, *Ri*, was used to assess water column stability due to stratification, and instability due to shear in the regions where thin layers were observed. Higher *Ri* values occurred in regions with higher N^2. The critical value $Ri = 0.25$ (equivalent to $\log_{10}Ri = -0.6$) is related to regions with high mixing potential due to shear instabilities. The $\mathrm{Log}_{10}Ri$ presented an average of 0.57 within the pycnocline, and 0.01 below the pycnocline (Table 2).

In Fig. 5e,f, the temporal distributions of N^2 are illustrated, with contours indicating the $\log_{10}Ri$ values, highlighting critical values ($\log_{10}Ri \leq -0.6$), to indicate the regions with intense mixing processes. On February 20th (Fig. 5e) higher values of $\log_{10}Ri$, between 1 and 1.5, occurred in the pycnocline region, where the N^2 values were higher. From the pycnocline the $\log_{10}Ri$ decreased toward the surface and the bottom. Negative values of $\log_{10}Ri$ probably occurred due

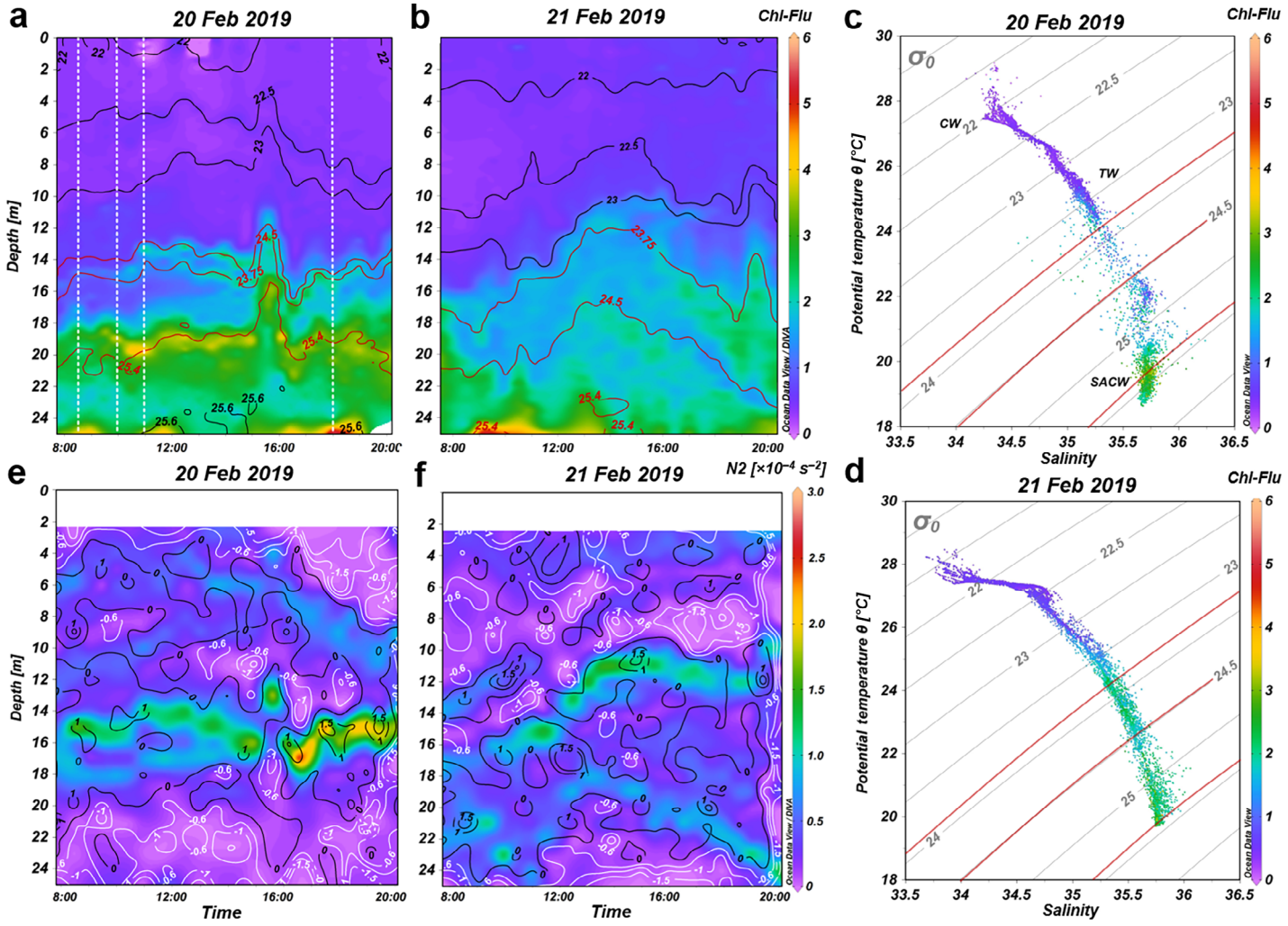

Fig 5. (**a**) Vertical distributions of chlorophyll *a* fluorescence (Chl-Flu) with isopycnal contours (σ_t black contours) over the day of Feb 20th; the dotted blank lines indicate the times when the profiles in Fig. 8 were collected. (**b**) Vertical distributions of Chl-Flu with isopycnal contours on Feb 21st. (**c**) TS-Chl-Flu diagram with isopycnals indicating water bodies on Feb 20th (CW = coastal water; TW = tropical water; SACW = South Atlantic central water). The red contours represent the 25.4, the 23.75 and the 24.5 isopycnals in the panels a and b, and in the T-S diagrams. (**d**) TS-Chl-Flu diagram on Feb 21st. (**e**) and (**f**) illustrate the vertical distributions of N^2 ($\times 10^{-4}$ s^{-2}) with $\log_{10}Ri$ contoured, on Feb 20th, and Feb 21st, respectively; white contours represent $\log_{10}Ri < -0.60$ (equivalent to $Ri < 0.25$). Data were plotted in Ocean Data View (Schlitzer, 2020).

to the influence of high shear near the surface, due to wind-driven mixing, and below 20 m depth, due to bottom friction. From 17:00 h, approximately, mixing processes along the water column intensified, indicated by values less than – 0.6.

Consecutive profiles of Chl-Flu and *Ri* (in terms of $\log_{10}Ri$) obtained between 08:30 h and 11:00 h on February 20th (Fig. 8a–c) showed that an initial Chl-Flu patch, between 19 and 21 m depth, increased in intensity and thinned as the *Ri* approached the critical value ($\log_{10}Ri = -0.6$). This indicates that the mechanism leading to thin layer formation in the region below the pycnocline was most likely related to shear. Around 15–16 m depth, Chl-Flu peaks were associated with $\log_{10}Ri > 1$, showing the strong influence of stratification within the pycnocline. In this case the observed thin layers were likely associated with both density stratification and current shear processes.

Thin layer dissipation

From 17:00 h on February 20th, the thin layers started to increase in vertical dimension (Fig. 5a), and on February 21st they had completely dissipated (Fig. 5b). Differences in weather and oceanographic conditions between February 20–21, 2019, are likely causes of the disappearance of the thin layers. The T-S diagram does not indicate the presence of SACW (Fig. 5d) on February 21st. The temperature ranged between 28.5°C, in the surface, and 19.8°C, near the bottom, and the salinity varied from 33.8, in the surface, to 36.0 near the bottom. In addition, the distribution of the $\log_{10}Ri$

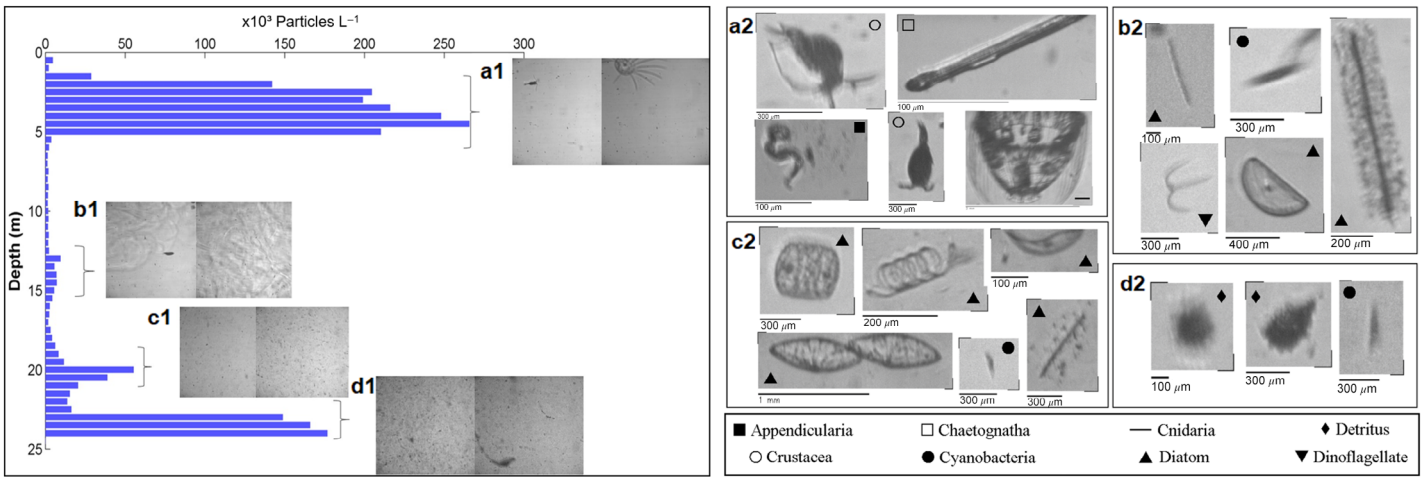

Fig 6. Vertical distribution of the average particle concentration (×10^3 Particles L^{-1}) captured by the imaging system on Feb 20th. (**a1**–**d1**) are full frames obtained by the system. (**a2**–**d2**) are examples of organisms from each corresponding region (a1–d1), obtained after the image segmentation and classification process. The taxonomic classification is indicated by the symbols (open square: Chaetognath; black square: Appendicularia; black line: Cnidaria; open dot: Crustacea; black dot: Cyanobacteria, black triangle: Diatom, upside-down triangle: Dinoflagellate; diamond: Detritus).

contours indicated high mixing potential throughout most of the water column (Fig. 5f). The average speed, V (cm s^{-1}), throughout the water column was 1.13 cm s^{-1} on February 20th, and 1.92 cm s^{-1} on February 21st (Table 3).

On February 20th, the current shear increased during the ebb tide. The shear through the entire water column averaged 0.51×10^{-4} s^{-2} during the flood tide and 0.56×10^{-4} s^{-2} during the ebb tide. Below the pycnocline (near the bottom), in general, there was an increase in the current shear in relation to the upper levels (within the pycnocline and in the mixed layer; Table 3). A small increase in current intensities and shear close to the bottom is shown in the vertical profiles of current vectors (Fig. 4).

The relaxation of the winds observed from the end of the day on February 20th (Fig. 3a), and change in wind direction on February 21st, caused an increase in the sea surface height by Ekman transport (Fig. 3b), and, consequently, the offshore advection of the SACW. Moreover, on February 21st there was an increase in current speed and shear, likely caused by the variability in the winds (Table 3). Thus, changes in the winds ultimately dissipated the thin layers observed on February 20th by driving the downwelling and the offshore advection of the nutrient-rich water mass, forcing changes in the vertical current distribution, and increasing the turbulent processes through the water column.

Discussion

Meteorological and oceanographic forcings and biological responses

Horizontal (or lateral) transport mediated by mesoscale and submesoscale processes is a major player in the dynamics of plankton populations, providing the basic mechanism for patchiness in the plankton distribution (Martin 2003). On the SBCS, the hydrodynamics are controlled primarily by winds, especially on the inner shelf, limited by the coast and by the 40–50 m isobaths. The South Atlantic Subtropical Anticyclone, the main feature of the atmospheric circulation over the South Atlantic Ocean, favors upwelling conditions on the SBCS during spring and summer months via Ekman transport, due to the predominant winds from the northeast (Castro et al. 2006). These meteorological and oceanographic conditions led to the presence of the SACW, a relatively cold (< 20°C) and nutrient-rich water body, close to the bottom, below 19.5 m depth (25 m total depth), on February 20th, 2019. Thin layers of phytoplankton with a Chl-Flu intensity ~ 2 times the background formed just below the pycnocline, coinciding with the upper limit of the SACW advection zone (Fig. 5a).

As SACW flows toward the coast in contact with the bottom layer, it is enriched with inorganic nutrients from the microbial mineralization of organic matter in the water column and in the sediments, acquiring high levels of nutrients, mainly nitrate (Braga and Müller 1998). The marine environment of the study area is meso-oligotrophic (Sassi and Kutner 1982). In such areas, primary productivity is strongly dependent on nutrients regenerated in the water and sediment, discharged by runoff from land or transported with oceanic water to the coast during upwelling events (Teixeira 1973).

Upon reaching the euphotic zone on the inner shelf, SACW often triggers phytoplankton blooms due to its enhanced nutrient levels (Aidar et al. 1993; Brandini 2006). For subtropical ecosystems of the southwestern Atlantic, the responses of the planktonic community to the enrichment of nutrients are well known, both for phytoplankton (Metzler et al. 1997; Saldanha-Corrêa and Gianesella 2004), and for zooplankton (Lopes et al. 2006; Marcolin et al. 2015; Melo

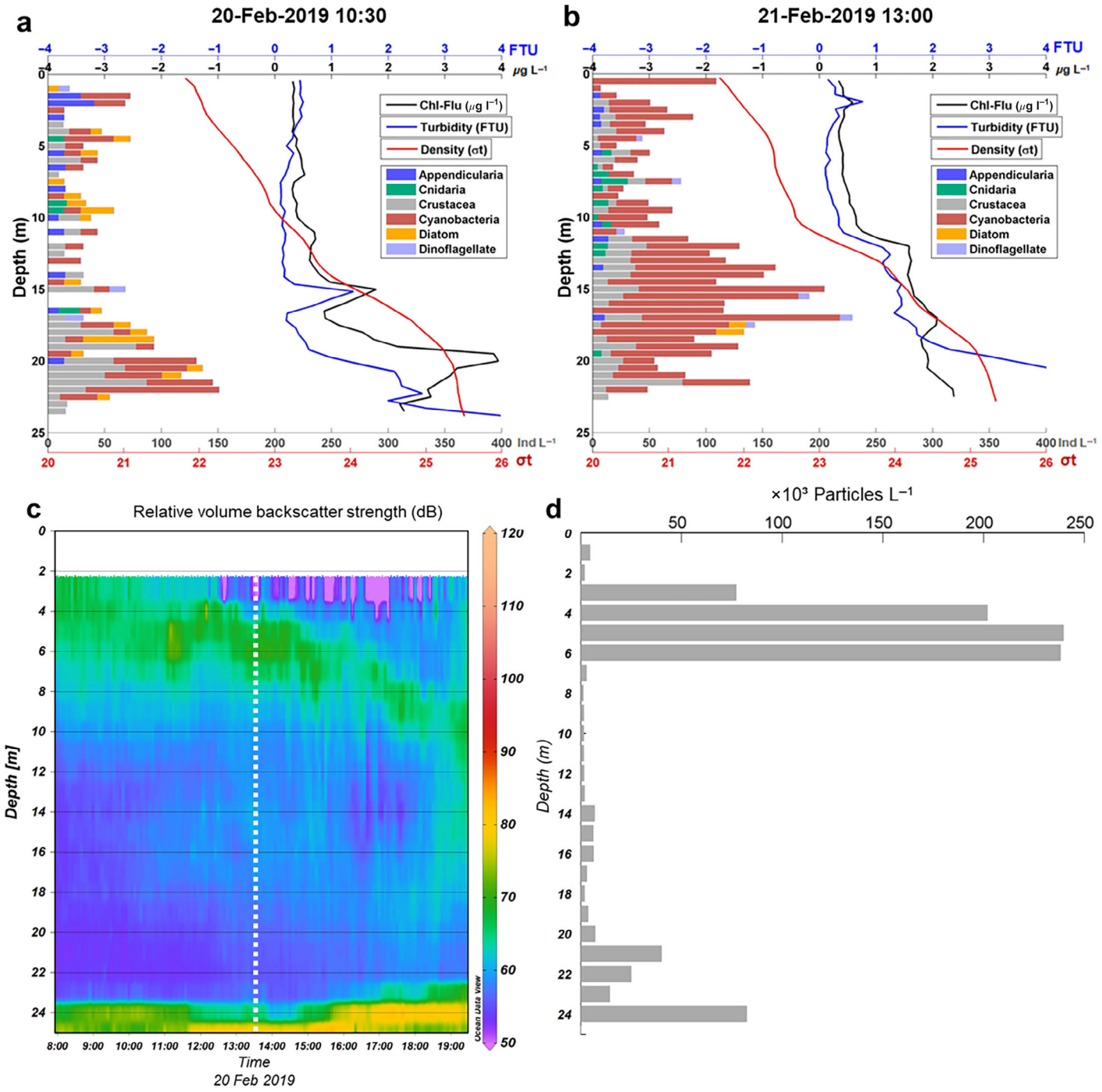

Fig 7. (**a**) Vertical distribution of individuals per liter of the main taxonomic groups found (bars; bottom-axis) and vertical profiles of Chl-Flu (black line; top-axis), turbidity (blue line; top-axis) and density (red line; bottom-axis), on Feb 20th at 10:30 h. (**b**) Vertical distribution of individuals per liter (bars; bottom-axis) and vertical profiles of Chl-flu (black line; top-axis), turbidity (blue line; top-axis) and density (red line; bottom-axis), on Feb 21st at 13:00 h. (**c**) Time distribution of the relative volume backscatter strength (RVBS, in dB); the dotted blank line indicate the time when the profile in the panel d was collected. (**d**) The particle distribution profile corresponding to time 13:30 h, on Feb 20th. Color legend in (a) is the same as in (b).

Júnior et al. 2016). However, until this contribution, the action of both physical and biological mechanisms on the formation of fine-scale phytoplankton aggregations had not been well documented.

Despite the quasi-synoptic sampling of this study (2 d), the mechanism that led to the formation of the phytoplankton-rich layer can be placed within a larger temporal context. We assume that the wind-driven mesoscale and submesoscale

Table 2. Average and median values for intensity, layer thickness, Brünt-Vaisala frequency N^2, shear S^2, and Richardson number ($\log_{10}Ri$), related to the thin layer depths for the three observed thin layers within and below the pycnocline on Feb 20th. The corresponding minimum (maximum) values are in parentheses, above (below) the average values.

	Intensity		Layer thickness (m)		N^2 ($\times 10^{-4}$ s^{-2})		S^2 ($\times 10^{-4}$ s^{-2})		$\log_{10}Ri$	
Layer location	**Average**	**Median**	**Average**	**Median**	**Average**	**Median**	**Average**	**Median**	**Average**	**Median**
Within the	(1.12)	2.12	(0.40)	1.00	(−0.13)	0.89	(0.07)	0.37	(−1.42)	0.40
pycnocline	2.12		0.85		0.96		0.46		0.57	
(n = 27)	(3.52)		(3.00)		(1.85)		(1.93)		(1.17)	
Below the	(2.39)	3.62	(0.80)	2.40	(−0.04)	0.12	(0.02)	0.89	(−2.40)	−0.29
pycnocline	3.62		2.27		0.14		0.34		0.01	
(n = 18)	(4.32)		(3.40)		(0.92)		(1.49)		(0.83)	

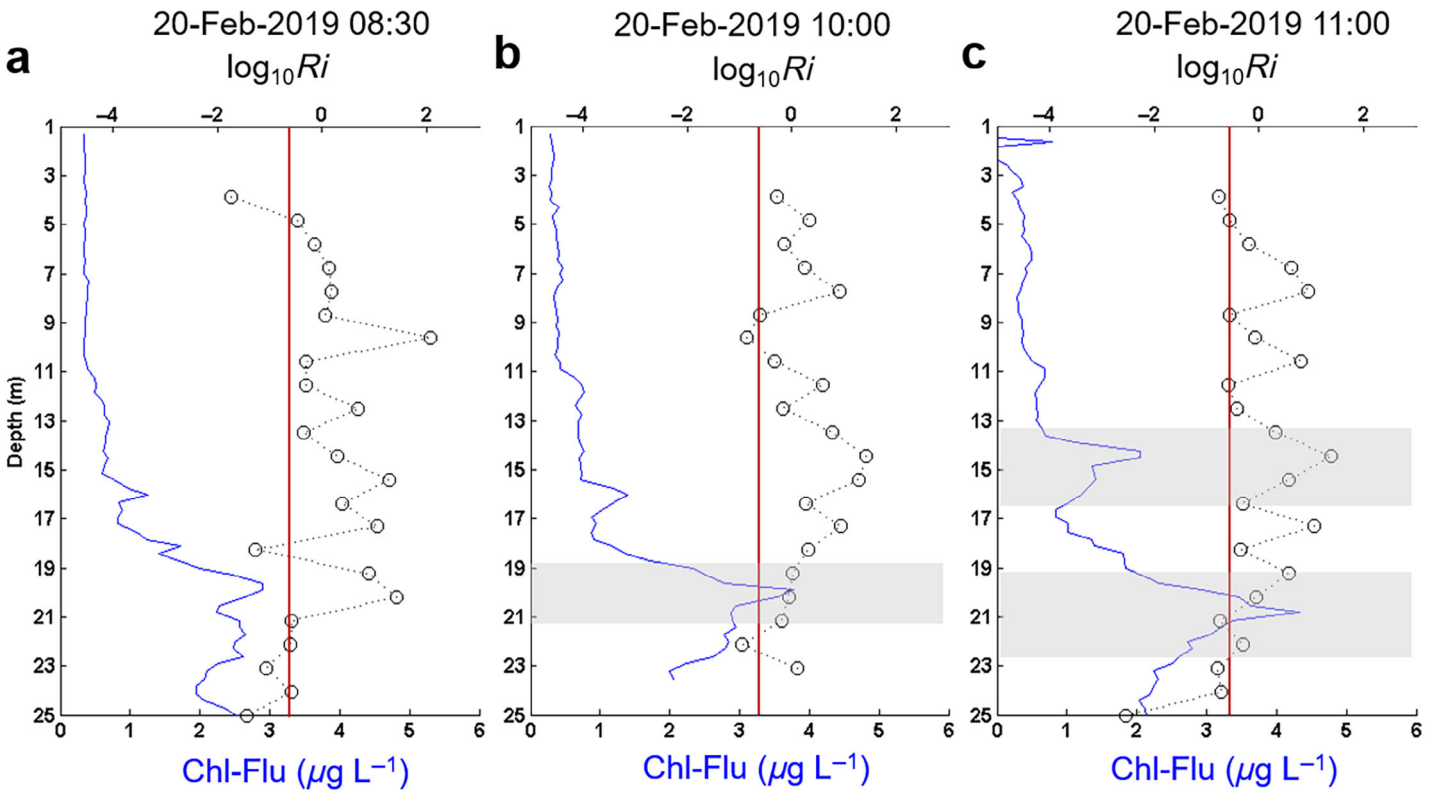

Fig 8. Chl-Flu (solid blue line) and $\log_{10}Ri$ (dotted line with open circles) profiles, obtained at the fixed-station point on Feb 20th at (**a**) 08:30 h, (**b**) 10:00 h, and (**c**) 11:00 h. The gray bars indicate the portions of the profile that met the criteria defining thin layers. The solid red lines indicate the critical value of $\log_{10}Ri = -0.60$ ($\log_{10}Ri < -0.60$ is equivalent to $Ri < 0.25$).

(1–500 km) processes allowed SACW to approach the coast, reaching the euphotic zone, and the phytoplankton responded to the availability of nutrients with in situ growth. The presence of SACW on the coast has a seasonal time scale, being more frequent from late spring to early autumn.

Regional meteorological and oceanographic conditions also acted in the dissipation of the phytoplankton layers. Between 08:00 h on February 20th and 20:00 h on February 21st, there was a relaxation in the upwelling winds (north-northeast winds < 3 m s^{-1}), and a subsequent increase in the winds from the southwest and southeast. These meteorological variations caused rapid changes in the water column, the sea surface height increased and favored coastal surface water downwelling, resulting in the SACW moving away from the coast. On February 21st, Chl-Flu was more evenly distributed and thin layers were absent.

Mechanisms of thin layer formation and dissipation

Several mechanisms have been posed leading to the formation of thin layers. In this work, the physical mechanisms of

Table 3. Average speed and average shear through the water column (3–25 m), mixed layer (3–11 m), through the pycnocline (12–18 m), and below the pycnocline to the bottom (19–25 m) for the flood and ebb tide periods, on Feb 20 and 21, 2019.

		V (cm s^{-1})		S^2 ($\times 10^{-4}$ s^{-2})			
				Flood tide		Ebb tide	
	Depth (m)	20/Feb	21/Feb	20/Feb	21/Feb	20/Feb	21/Feb
Mixed layer	3–11	1.18	2.10	0.57	0.59	0.65	0.54
Pycnocline	12–18	1.14	2.08	0.33	0.49	0.36	0.44
Below pycnocline	19–25	1.07	1.50	0.61	0.56	0.66	0.59
Water column	3–25	1.13	1.92	0.51	0.55	0.56	0.53

stratification and vertical current shear will be specifically discussed. Fluid stratification can cause organisms and biogenic materials (e.g., marine snow) to establish at certain depths based on density gradients (Prairie and White 2017). Large plankton patches can become thinner by vertical shear due to current jets, internal waves and horizontal intrusion (Eckart 1948; Ryan et al. 2008; Durham and Stocker 2012). Phytoplankton motility can also act to form thin layers (Stacey et al. 2007; Durham and Stocker 2012).

Strong vertical density stratification was established on February 20th, with density (σ_t) ranging from 21.8 in the surface to 25.6 in the bottom. Thin phytoplankton layers were observed in different depths in the water column. Sixty percent of the recorded chlorophyll peaks were associated with high stability within the pycnocline (~ 14.5–16.0 m depth) with average $N^2 = 0.96 \times 10^{-4}$ s^{-2}. Forty percent of the Chl *a* peaks formed below the pycnocline (~ 19–21 m depth), in a relatively cold water zone (~ 19°C), with an average $N^2 = 0.14 \times 10^{-4}$ s^{-2} (Table 2).

Although with low values, the vertical current shear was present in the depths of the thin layers on February 20th. Vertical profiles of horizontal currents indicate vertical shear at medium depths (~ 14.5, 16, and 20 m) where thin layers were observed (Fig. 4a1). However, no thin layers were observed in regions with values of $Ri < 0.25$—critical value that signals regions with high turbulent processes due to shear. Dekshenieks et al. (2001) found no thin layers when $Ri < 0.23$, which was probably due to the dissipation caused by the turbulence.

Consecutive profiles, obtained between 8:00 h and 11:00 h on February 20th, allowed us to observe that as the $\log_{10}Ri$ approached critical values (– 0.6, i.e., $Ri = 0.25$), a Chl-Flu patch located below the pycnocline (~ 19–21 m) decreased in the vertical scale (thickness) and increased in intensity (Fig. 8a–c). This suggests that the increase in current shear resulted in the phytoplankton layer thinning at this depth, a mechanism known as *straining* (Durham and Stocker 2012). Ryan et al. (2008) indicated shear as a convergent process (forming thin layers) in a coastal upwelling system (Monterey Bay), in 2003, where 92% of the thin layers recorded were associated with shear peaks.

Over this same sequence of profiles (Fig. 8a–c), for thin layers located in the pycnocline (~ 14.5–16.0 m), the $\log_{10}Ri$ values remained greater than 1, while the Chl-Flu peak increased, indicating a greater influence of the stratification in this region. The thin layers that had formed within the pycnocline followed two isopycnals ($\sigma_t = 24.5$ and $\sigma_t = 23.75$), suggesting that the phytoplankton could be composed of motile cells in these layers (Ryan et al. 2010; Durham and Stocker 2012). The results of the imaging system indicate the presence of motile dinoflagellate cells of the genus *Ceratium* and colonies of *Chaetoceros coarctatus* with their motile *Vorticella* epibionts in this region (around 15 m) (Fig. 6b2). Stratification may have driven the establishment of phytoplankton in a specific density gradient according to cell buoyancy. The shear probably acted to form thin layers at this depth, by interrupting the vertical movement of cells through the fluid, trapping them in the form of thin layers, the mechanism known as *gyrotactic trapping* (Hoecker-Martínez and Smyth 2012). The thin layers below the pycnocline followed a single isopycnal ($\sigma_t = 25.4$) during the study period, indicating that the cells did not move vertically. Image classification results revealed filamentous cyanobacteria and many species of diatoms in this depth (19–21 m) (Fig. 6c2). Although some *C. coarctatus* were found in this layer depth, most diatoms were nonmotile cells.

Mechanisms of thin layer formation triggered by shear have been pointed out in several studies (Dekshenieks et al. 2001; Stacey et al. 2007; Hoecker-Martínez and Smyth 2012). Even though the shear values were underestimated by Ryan et al. (2008) by the coarse sampling scale (meter-scale), it was possible to identify shear as the main mechanism for the formation of thin layers observed in their study. The results of our study imply that differencing levels of shear acted both as a convergent process in the formation of thin layers, and as a divergent process leading to the dissipation of thin layers at the end of February 20th and throughout February 21st.

On February 21st, the average current speed almost doubled in value through the pycnocline between 12 and 18 m (2.08 cm s^{-1}) compared to the previous day (1.14 cm s^{-1}) (Table 3). Higher shear values were obtained in both flood and ebb tide periods through the water column ($S^2 = 0.55 \times 10^{-4}$ s^{-2}

and $S^2 = 0.53 \times 10^{-4}$ s^{-2}, respectively). In addition, a water column with a higher mixing potential was evidenced by the more widespread distribution of critical values ($Ri < 0.25$). No thin layers were observed under these conditions, probably due to decreased stability. According to Dekshenieks et al. (2001), persistent thin layers are not expected in regions under tidal mixing, nor in surface layers subject to wind stress. That is, in regions of instability and active mixing, the maintenance of these structures is impaired and there is a greater tendency to dissipate.

The current speed had intensities in the order of centimeters per second, which is consistent with the typical tidal currents (suprainertial) on the continental shelf of the study region (Alves 1992). Although tidal regimes in coastal and shallow areas can act strongly in the mixing of the water column, the tide is not considered the most energetic forcing in this region, but the wind is. The ocean circulation response to the wind field variability, in the inner and midshelf regions, can occur practically in phase with the wind, as the local forcing is dominant in highly frictional regimes (Csanady 1978).

Vertical distribution of particles and plankton

Studying the distribution of plankton organisms in their natural environment and their behavior in relation to thin layers is of crucial importance to assess the ecological impact of these structures. Imaging systems have been used to document the relationships between thin layers of phytoplankton and higher trophic levels (Möller et al. 2012; Talapatra et al. 2013). Here images were used quantitatively and qualitatively to analyze the distribution of microplankton and mesoplankton, generating an overview of the main classes present in the vicinity of the phytoplankton layers and through the water column.

In the images collected in the location of the thin layers, on February 20th, dinoflagellates, diatoms and cyanobacteria were identified. In the depths between 13 and 16 m, within the pycnocline, dinoflagellate species of the genus *Ceratium* were found (Fig. 6b2). Species of *Ceratium* are mixotrophic, that is, they are both photosynthetic and heterotrophic, feeding on other plankton. They belong to the microplankton (20–200 μm), but some species can reach more than 200 μm in length. Most dinoflagellates are motile cells during their planktonic stage and can migrate vertically (Baek et al. 2009). This may explain why the thin layers found in this depth range appeared to move vertically between two isopycnals.

Some species of large diatoms (> 200 μm) were identified in the depths between 19 and 21 m, mostly nonmotile species, and many filaments of the cyanobacteria *Trichodesmium erythraeum* (Fig. 6c2). Although *Trichodesmium* and the large diatoms contribute to Chl-*a* fluorescence, the Chl-Flu peaks may also had been composed mainly of phytoplankton less than 100 μm in length, which were not considered in the image classification stage. In addition, small diatoms and dinoflagellates from the picophytoplankton and nanophytoplankton (< 20 μm fractions) make up a large part of the plankton in the study area (Villac et al. 2008) and could not be identified using the imaging system. The organisms in the fraction > 20 μm were estimated in the general particle count, which indicated aggregations of particles at depths coinciding with the locations of the thin layers.

A higher density of crustaceans was found in the vicinity of Chl-Flu peaks on February 20th. A major representative of crustaceans in the region are copepods (Melo Júnior et al. 2016), which feed on phytoplankton, but are mostly omnivorous (Turner 2004). Marcolin et al. (2015) employed an Laser Optical Particle Counter (LOPC) to study the distribution of marine particles and mesozooplankton, on the Brazilian coast, finding positive correlations between chlorophyll fluorescence and particle aggregates, and between Brunt-Väisälä frequency (N^2) and particle aggregates; peaks of zooplankton and aggregate concentration usually coincided with each other and with the pycnocline.

Appendicularians and cnidarians were found in greater quantities close to the surface (0–3 m) and subsurface (3–10 m) on both days. The presence of these two groups was also verified close to the Chl-Flu peaks (between 14.5–16 m and 19–21 m) on February 20th (Fig. 7a). Large concentrations of appendicularians close to the surface have been reported previously in the region. Marcolin et al. (2015) found appendicularians peaks near the surface and below 20 m on the inner shelf off Ubatuba, in 5-yr time series data, from 2007 to 2012. In this same region, Miyashita and Lopes (2011) found the most abundant appendicularian species above the thermocline and in surface layers, where high temperatures and low Chl-*a* prevailed. Appendicularians are free-swimming, solitary, herbivorous tunicates, feeding primarily on nanoplankton-sized particles using a "house" secreted by the glandular epithelium. The images indicated that several appendicularians were without their mucus houses, probably due to the sensitivity of these structures to the increased turbulence and friction of the currents in the mixed layer. Appendicularians are an important link between pico-nanoplankton and higher trophic levels since they are part of the diet of fish, cnidarians, ctenophores and chaetognaths (Urban-Rich et al. 2006). Cnidarians are free-living carnivorous that feed on various species, from microscopic zooplankton to small fish. Feeding behavior is regulated by chemosensors, and they move through the water column in search of food (Miglietta et al. 2000). The presence of cnidarians in the mixed layer and close to the peaks of Chl-Flu can be related to the presence of appendicularians and crustaceans.

On February 21st, there was a significant increase in the density of cyanobacteria through the water column, especially in midwater (11–20 m), accompanying the increase in Chl-Flu (Fig. 7b). Previous studies have reported blooms of *Trichodesmium* spp. on the southeastern coast of Brazil (Carvalho et al. 2008; Detoni et al. 2016). The maximum *Trichodesmium* abundances were associated in previous studies

with local enrichments of phosphate, iron, or both (Fernández et al. 2010; Detoni et al. 2016), high surface temperatures (Carvalho et al. 2008) and salinity range between 33 and 37 (Fu and Bell 2003). In situations where there is a strong thermal stratification and a shallow mixed layer, phytoplankton groups that demonstrate rapid growth under conditions of abundant nutrients (mainly phosphate and iron) can be overcome by *Trichodesmium* (Chen et al. 2008). On the days leading up to the *Trichodesmium* bloom on February 21st, the weather conditions were stable, with calm sea and a smooth water surface, weak winds (< 11 m s^{-1}) and partly cloudy skies. Thermal stratification of the water column was observed on February 20th, with the temperature ranging from 29°C on the surface to 18.6°C on the bottom layer, and the salinity ranging from 34 to 36.5. These characteristics, together with the high relative concentration of phosphate (> 0.12 μM) likely triggered the population growth of *Trichodesmium erythraeum*.

Based on the hypothesis that particles are transported passively by water bodies and they move together at the same speed, ADCPs use the backscattered sound by particles suspended in water to measure the velocity of currents. From the measurements of vertical velocity and echo intensity (signal strength), ADCPs have been used in the investigation of zooplanktonic biomass (Sevadjian et al. 2010; Comfort et al. 2017). The ADCP signal strength was used to estimate the number of particles suspended from the RVBS calculation. Because acoustic waves are reflected by all objects greater than ¼ of the pulse wavelength, it is not possible to determine exactly how much of the reflected signal is due to zooplankton (Thomson and Emery 2014). In our case, the wavelength of the sound pulses is about 0.3 cm (considering the sound speed in seawater of 1475 m s^{-1} and the ADCP frequency of 500 kHz), meaning that, in general, particles larger than 750 μm reflect the sound, and the smaller than 750 μm scatter the sound. However, the signal strength is proportional to the aggregation of the organisms. Organisms that are aggregated into patches have a greater volume scattering strength than uniform distributions of the same zooplankton organisms (Thomson and Emery 2014).

The RVBS distribution graph suggests a patch of particles in the subsurface layer (~ 3–6 m) (Fig. 7c). As zooplankton swarms tend to aggregate at specific depths (Guerra et al. 2019), the higher intensity of RVBS may indicate the detection of a zooplankton layer in this region. Mesozooplankton organisms such as appendicularians, cnidarians and chaetognaths, were detected by the imaging system in this depth range. In addition, the particle counts from the imaging system also revealed a higher particle concentration in the subsurface layer (Fig. 7d).

Physical-biological coupling in Ubatuba—concluding remarks

This contribution describes coupled biological-physical processes leading to the presence of thin layers in the coastal region of Ubatuba, Brazil. We demonstrated that the occurrence and persistence of thin layers were conditioned by the variability of hydrographic conditions through the water column. The dynamic processes in quasi-synoptic scale influenced the fine-scale physical processes of stratification and current shear, which influenced biological processes, such as the accumulation of phytoplankton biomass. Although the observation of the phenomenon was local, the entire region of the SBCS has its circulation controlled by the same meteorological conditions on a synoptic scale, according to Castro Filho et al. (1987). The thin layers observed are associated with mesoscale and submesoscale flows, related to Ekman transport and the advection of water bodies in the coastal zone. Thus, the observed changes are likely to occur at the regional level and are representative of similar coastal ecosystems.

The higher concentration of organisms found in the thin layer depths, compared to the environment above and below the layers, indicates that thin phytoplankton layers are likely attractive food sources for grazers. The importance of thin phytoplankton layers as enhanced feeding grounds for consumers that migrate to the vicinity of the layers has been well documented (Benoit-Bird et al. 2010; Greer et al. 2013). As trophic hotspots, thin layers of phytoplankton can mediate the survival and reproduction rates of organisms belonging to higher trophic levels (Durham and Stocker 2012).

We conclude that thin layers on the inner shelf of Ubatuba have a transitory nature, influenced by regional winds and intermittent SACW intrusions from the outer shelf, and their occurrence contributes to the ecological function of this ecosystem. Future research projects would require sampling strategies targeting fine-resolution spatial and temporal scales, with improved multifrequency acoustic and direct sampling methods. Studies on thin biological layers in the South Atlantic are still incipient and there are many questions to be answered, such as the influence of nonlinear internal waves on the occurrence of thin layers, and the role of thin layers in fish and zooplankton feeding processes. Future studies that quantify the phytoplankton taxa and size classes exploited by zooplankton in thin layers will help to better assess the ecological role that these structures play in meso-oligotrophic coastal environments.

References

Aidar, E., S. A. Gaeta, S. M. F. Gianesella-Galvão, M. B. B. Kutner, and C. Teixeira. 1993. Ecossistema costeiro subtropical: nutrientes dissolvidos, fitoplâncton e clorofila-a e suas relações com as condições oceanográficas na região de Ubatuba, SP. Publ. Esp. Inst. Oceanogr. **10**: 9–43.

Alves, M. A. 1992. Correntes de Maré e Inerciais na Plataforma Continental ao Largo de Ubatuba (SP). Master's thesis. Univ. of São Paulo, Oceanographic Institute.

Baek, S. H., S. Shimode, K. Shin, M. S. Han, and T. Kikuchi. 2009. Growth of dinoflagellates, *Ceratium furca* and *Ceratium fusus* in Sagami Bay, Japan: The role of vertical

migration and cell division. Harmful Algae **8**: 843–856. doi:10.1016/j.hal.2009.04.001

Barnett, M. L., A. E. Kemp, A. E. Hickman, and D. A. Purdie. 2019. Shelf Sea subsurface chlorophyll maximum thin layers have a distinct phytoplankton community structure. Cont. Shelf Res. **174**: 140–157. doi:10.1016/j.csr.2018.12.007

Batista, S. S., and J. Harari. 2017. Modeling of the dispersion of thermotolerant coliforms and enterococci in two bays in the coastal region of Ubatuba (SP), Brazil. Eng. Sanit. Ambient. **22**: 403–413. doi:10.1590/s1413-41522016158594

Benoit-Bird, K. J., T. J. Cowles, and C. E. Wingard. 2009. Edge gradients provide evidence of ecological interactions in planktonic thin layers. Limnol. Oceanogr. **54**: 1382–1392. doi:10.4319/lo.2009.54.4.1382

Benoit-Bird, K. J., M. A. Moline, C. M. Waluk, and I. C. Robbins. 2010. Integrated measurements of acoustical and optical thin layers I: Vertical scales of association. Cont. Shelf Res. **30**: 17–28. doi:10.1016/j.csr.2009.08.001

Bochdansky, A. B., S. M. Bollens, G. C. Rollwagen-Bollens, and A. H. Gibson. 2010. Effect of the heterotrophic dinoflagellate *Oxyrrhis marina* and the copepod *Acartia tonsa* on vertical carbon flux in and around thin layers of the phytoflagellate *Isochrysis galbana*. Mar. Ecol. Prog. Ser. **402**: 179–196. doi:10.3354/meps08428

Braga, E. D. S., and T. J. Müller. 1998. Observation of regeneration of nitrate, phosphate and silicate during upwelling off Ubatuba, Brazil, 23°S. Cont. Shelf Res. **18**: 915–922. doi:10.1016/S0278-4343(98)00002-8

Brandini, F. P. 2006. Hidrografia e Produção Biológica na região Sudeste-Sul do Brasil no contexto do Programa REVIZEE, p. 447–460. *In* O Ambiente oceanográfico da plataforma continental e do talude na região sudeste-sul do Brasil. Edusp. São Paulo.

Breckenridge, J. K., and S. M. Bollens. 2010. Biological thin layer formation: Interactions between the larval decapod, *Neotrypaea californiensis*, haloclines and light. J. Plankton Res. **32**: 1097–1102. doi:10.1093/plankt/fbq035

Carvalho, M., S. M. Gianesella, and F. M. Saldanha-Corrêa. 2008. *Trichodesmium erythraeum* bloom on the continental shelf off Santos, Southeast Brazil. Braz. J. Oceanogr. **56**: 307–311. doi:10.1590/S1679-87592008000400006

Castro Filho, B. M., L. B. D. Miranda, and S. Y. Miyao. 1987. Hydrographic conditions on the continental shelf off Ubatuba: Seasonal and meso-scale variability. Bol. Inst. Oceanogr. **35**: 135–151. doi:10.1590/S0373-55241987000200004

Castro, B. M., and T. N. Lee. 1995. Wind-forced sea level variability on the southeast Brazilian shelf. J. Geophys. Res.: Oceans **100**: 16045–16056. doi:10.1029/95JC01499

Castro, B. M., J. A. Lorenzetti, I. C. A. Silveira, and L. B. Miranda. 2006. Estrutura termohalina e circulação na região entre o Cabo de São Tomé (RJ) e o Chuí (RS), p. 11–120. *In* O Ambiente Oceanográfico da Plataforma Continental e do Talude na Região Sudeste-Sul do Brasil. Edusp.

Chassot, E., S. Bonhommeau, N. K. Dulvy, F. Mélin, R. Watson, D. Gascuel, and O. Le Pape. 2010. Global marine primary production constrains fisheries catches. Ecol. Lett. **13**: 495–505. doi:10.1111/j.1461-0248.2010.01443.x

Chen, Y. L. L., H. Y. Chen, S. H. Tuo, and K. Ohki. 2008. Seasonal dynamics of new production from Trichodesmium N2 fixation and nitrate uptake in the upstream Kuroshio and South China Sea basin. Limnol. Oceanogr. **53**: 1705–1721. doi:10.4319/lo.2008.53.5.1705

Cheriton, O. M., M. A. McManus, D. V. Holliday, C. F. Greenlaw, P. L. Donaghay, and T. J. Cowles. 2007. Effects of mesoscale physical processes on thin zooplankton layers at four sites along the west coast of the U.S. Estuar. Coasts **30**: 1–16. doi:10.1007/BF02841955

Comfort, C., K. Smith, M. A. McManus, A. Neuheimer, J. Sevadjian, and C. Ostrander. 2017. Observations of the Hawaiian mesopelagic boundary layer community in daytime and nighttime habitats using estimated backscatter. AIMS Geosci. **3**: 304–326. doi:10.3934/geosci.2017.3.304

Cowles, T. J., R. A. Desiderio, and M. E. Carr. 1998. Small-scale planktonic structure: Persistence and trophic consequences. Oceanography **11**: 4–9. doi:10.5670/oceanog.1998.08

Csanady, G. T. 1978. Wind effects on surface to bottom fronts. J. Geophys. Res.: Oceans **83**: 4633–4640. doi:10.1029/JC083iC09p04633

De Verneil, A., P. J. S. Franks, and M. D. Ohman. 2019. Frontogenesis and the creation of fine-scale vertical phytoplankton structure. J. Geophys. Res.: Oceans **124**: 1509–1523. doi:10.1029/2018JC014645

Deines, K. L. 1999. Backscatter estimation using broadband acoustic Doppler current profilers, p. 249–253. *In* Proceedings of the IEEE Sixth Working Conference on Current Measurement (Cat. No. 99CH36331). IEEE. doi:10.1109/CCM.1999.755249

Dekshenieks, M. M., P. L. Donaghay, J. M. Sullivan, J. E. B. Rines, T. R. Osborn, and M. S. Twardowski. 2001. Temporal and spatial occurrence of thin phytoplankton layers in relation to physical processes. Mar. Ecol. Prog. Ser. **223**: 61–71. doi:10.3354/meps223061

Detoni, A. M. S., Á. M. Ciotti, P. H. Calil, V. M. Tavano, and J. S. Yunes. 2016. *Trichodesmium* latitudinal distribution on the shelf break in the southwestern Atlantic Ocean during spring and autumn. Global Biogeochem. Cycles **30**: 1738–1753. doi:10.1002/2016GB005431

Donaghay, P. L., H. M. Rines, and J. M. Sieburth. 1992. Simultaneous sampling of fine scale biological, chemical, and physical structure in stratified waters. Arch. Hydrobiol. Beih. Ergebn. Limnol. **36**: 97–108.

Durham, W. M., and R. Stocker. 2012. Thin phytoplankton layers: Characteristics, mechanisms, and consequences. Ann. Rev. Mar. Sci. **4**: 177–207. doi:10.1146/annurev-marine-120710-100957

Eckart, C. 1948. An analysis of the stirring and mixing processes in incompressible fluids. J. Mar. Res. **7**: 265–275.

Fernández, A., B. Mouriño-Carballido, A. Bode, M. Varela, and E. Marañón. 2010. Latitudinal distribution of *Trichodesmium* spp. and N2 fixation in the Atlantic Ocean. Biogeosciences **7**: 3167–3176. doi:10.5194/bg-7-3167-2010

Fu, F. X., and P. R. F. Bell. 2003. Effect of salinity on growth, pigmentation, N2 fixation and alkaline phosphatase activity of cultured *Trichodesmium* sp. Mar. Ecol. Prog. Ser. **257**: 69–76. doi:10.3354/meps257069

Greer, A. T., R. K. Cowen, C. M. Guigand, M. A. McManus, J. C. Sevadjian, and A. H. V. Timmerman. 2013. Relationships between phytoplankton thin layers and the fine-scale vertical distributions of two trophic levels of zooplankton. J. Plankton Res. **35**: 939–956. doi:10.1093/plankt/fbt056

Guerra, D., K. Schroeder, M. Borghini, E. Camatti, M. Pansera, A. Schroeder, S. Sparnocchia, and J. Chiggiato. 2019. Zooplankton diel vertical migration in the Corsica Channel (North-Western Mediterranean Sea) detected by a moored acoustic Doppler current profiler. Ocean Sci. **15**: 631–649. doi:10.5194/os-15-631-2019

Harari, J., and A. R. Mesquita. 2003. Tábuas das marés de Ubatuba, Santos e Cananéia para os anos de 2004 e 2005. Relat. Inst. Oceanogr. **51**: 1–28.

Hoecker-Martínez, M. S., and W. D. Smyth. 2012. Trapping of gyrotactic organisms in an unstable shear layer. Cont. Shelf Res. **36**: 8–18. doi:10.1016/j.csr.2012.01.003

Itsweire, E. C., T. R. Osborn, and T. P. Stanton. 1989. Horizontal distribution and characteristics of shear layers in the seasonal thermocline. J. Phys. Oceanogr. **19**: 301–320. doi:10.1175/1520-0485(1989)019<0301:HDACOS>2.0.CO;2

Lopes, R. M., M. Katsuragawa, J. F. Dias, M. A. Montú, J. H. Muelbert, C. Gorri, and F. P. Brandini. 2006. Zooplankton and ichthyoplankton distribution on the southern Brazilian shelf: An overview. Sci. Mar. **70**: 189–202. doi:10.3989/scimar.2006.70n2189

Marcolin, C. R., S. Gaeta, and R. M. Lopes. 2015. Seasonal and interannual variability of zooplankton vertical distribution and biomass size spectra off Ubatuba, Brazil. J. Plankton Res. **37**: 808–819. doi:10.1093/plankt/fbv035

Martin, A. P. 2003. Phytoplankton patchiness: The role of lateral stirring and mixing. Prog. Oceanogr. **57**: 125–174. doi:10.1016/S0079-6611(03)00085-5

Mazzini, P. L. F. 2009. Subdital inner-shelf currents between Peruíbe and São Sebastião: Observations. Master's thesis. Univ. of São Paulo, Oceanographic Institute. 10.11606/D.21.2009.tde-22092009-154153

McManus, M. A., R. M. Kudela, M. W. Silver, G. F. Steward, P. L. Donaghay, and J. M. Sullivan. 2008. Cryptic blooms: Are thin layers the missing connection? Estuar. Coasts **31**: 396–401. doi:10.1007/s12237-007-9025-4

McManus, M., J. C. Sevadjian, K. J. Benoit-Bird, O. M. Cheriton, A. H. V. Timmerman, and C. M. Waluk. 2012. Observations of thin layers in coastal Hawaiian waters. Estuar. Coasts **35**: 1119–1127. doi:10.1007/s12237-012-9497-8

Medeiros, M. 2017. Development of an in situ image capture instrumentation to study the vertical distribution of plankton. Master's thesis. Univ. of São Paulo, Oceanographic Institute. 10.11606/D.21.2018.tde-21032018-150041

Melo Júnior, M., C. R. Marcolin, L. K. Miyashita, and R. M. Lopes. 2016. Temporal changes in pelagic copepod assemblages off Ubatuba, Brazil. Mar. Ecol. **37**: 877–890. doi:10.1111/maec.12366

Mesquita, A. R. D., and J. Harari. 1983. Tides and tide gauges of Cananéia and Ubatuba-Brazil (lat, 24). Relat. Inst. Oceanogr. **11**: 1–14.

Metzler, P. M., P. M. Glibert, S. A. Gaeta, and J. M. Ludlamt. 1997. New and regenerated production in the South Atlantic off Brazil. Deep-Sea Res. I Oceanogr. Res. Pap. **44**: 363–384. doi:10.1016/S0967-0637(96)00129-X

Miglietta, M. P., L. Della Tommasa, F. Denitto, C. Gravili, P. Pagliara, J. Bouillon, and F. Boero. 2000. Approaches to the ethology of hydroids and medusae (Cnidaria, Hydrozoa). Sci. Mar. **64**: 63–71. doi:10.3989/scimar.2000.64s163

Miranda, L. B., and M. Katsuragawa. 1991. Estrutura térmica na região sudeste do Brasil (outubro/novembro de 1988). Publ. Esp. Inst. Oceanogr. **8**: 1–14.

Miyashita, L. K., and R. M. Lopes. 2011. Larvacean (Chordata, Tunicata) abundance and inferred secondary production off southeastern Brazil. Estuar. Coast. Shelf Sci. **92**: 367–375. doi:10.1016/j.ecss.2011.01.007

Möller, K. O., M. S. John, A. Temming, J. Floeter, A. F. Sell, J. P. Herrmann, and C. Möllmann. 2012. Marine snow, zooplankton and thin layers: Indications of a trophic link from small-scale sampling with the video plankton recorder. Mar. Ecol. Prog. Ser. **468**: 57–69. doi:10.3354/meps09984

Mullin, M. M., and E. R. Brooks. 1976. Some consequences of distributional heterogeneity of phytoplankton and zooplankton. Limnol. Oceanogr. **21**: 784–796. doi:10.4319/lo.1976.21.6.0784

Onitsuka, G., Y. Yoshikawa, T. Shikata, K. Yufu, K. Abe, T. Tokunaga, K. Kimoto, and T. Matsuno. 2018. Development of a thin diatom layer observed in a stratified embayment in Japan. J. Oceanogr. **74**: 351–365. doi:10.1007/s10872-018-0466-0

Pond, S., and G. L. Pickard. 1983. Introductory dynamical oceanography, 2nd ed. Oxford: Butterworth-Heinemann.

Prairie, J. C., and B. L. White. 2017. A model for thin layer formation by delayed particle settling at sharp density gradients. Cont. Shelf Res. **133**: 37–46. doi:10.1016/j.csr.2016.12.007

Reboita, M. S., T. Ambrizzi, B. Silva, R. Pinheiro, and R. P. Da Rocha. 2019. The South Atlantic subtropical anticyclone: Present and future climate. Front. Earth Sci. **7**: 8. doi:10.3389/feart.2019.00008

Roemmich, D., and J. McGowan. 1995. Climatic warming and the decline of zooplankton in the California current. Science **267**: 1324–1326. doi:10.1126/science.267.5202.1324

Ryan, J. P., M. A. McManus, J. D. Paduan, and F. P. Chavez. 2008. Phytoplankton thin layers caused by shear in frontal zones of a coastal upwelling system. Mar. Ecol. Prog. Ser. **354**: 21–34. doi:10.3354/meps07222

Ryan, J. P., M. A. McManus, and J. M. Sullivan. 2010. Interacting physical, chemical and biological forcing of phytoplankton thin-layer variability in Monterey Bay, California. Cont. Shelf Res. **30**: 7–16. doi:10.1016/j.csr.2009.10.017

Ryan, J. P., et al. 2014. Boundary influences on HAB phytoplankton ecology in a stratification-enhanced upwelling shadow. Deep-Sea Res. Part II: Top. Stud. Oceanogr. **101**: 63–79. doi:10.1016/j.dsr2.2013.01.017

Saldanha-Corrêa, F. M. P., and S. M. F. Gianesella. 2004. A microcosm approach on the potential effects of the vertical mixing of water masses over the primary productivity and phytoplankton biomass in the southern Brazilian coastal region. Braz. J. Oceanogr. **52**: 167–182. doi:10.1590/S1679-87592004000300001

Sassi, R., and M. B. B. Kutner. 1982. Variação sazonal do fitoplâncton da região do Saco da Ribeira, Ubatuba, Brasil. Bol. Inst. Oceanogr. **31**: 29–42. doi:10.1590/S0373-55241982000200005

Schlitzer, R. 2020. Ocean Data View. https://odv.awi.de

Sevadjian, J. C., M. A. McManus, and G. Pawlak. 2010. Effects of physical structure and processes on thin zooplankton layers in Mamala Bay, Hawaii. Mar. Ecol. Prog. Ser. **409**: 95–106. doi:10.3354/meps08614

Shroyer, E. L., K. J. Benoit-Bird, J. D. Nash, and J. N. Mou. 2014. Stratification and mixing regimes in biological thin layers over the mid-Atlantic bight. Limnol. Oceanogr. **59**: 1349–1363. doi:10.4319/lo.2014.59.4.1349

SonTek. 1997. SonTek Doppler current meters—using signal strength to monitor suspended sediment concentration. San Diego: SonTek Application Notes.

Stacey, M. T., M. A. McManus, and J. V. Steinbuck. 2007. Convergences and divergences and thin layer formation and maintenance. Limnol. Oceanogr. **52**: 1523–1532. doi:10.4319/lo.2007.52.4.1523

Steinbuck, J. V., M. T. Stacey, M. A. McManus, O. M. Cheriton, and J. P. Ryan. 2009. Observations of turbulent mixing in a phytoplankton thin layer: Implications for formation, maintenance, and breakdown. Limnol. Oceanogr. **54**: 1353–1368. doi:10.4319/lo.2009.54.4.1353

Stewart, R. H. 2008. Introduction to physical oceanography. College Station: Texas A&M University.

Sullivan, J. M., P. L. Donaghay, and J. E. B. Rines. 2010. Coastal thin layer dynamics: Consequences to biology and optics. Cont. Shelf Res. **30**: 50–65. doi:10.1016/j.csr.2009.07.009

Talapatra, S., and others. 2013. Characterization of biophysical interactions in the water column using in situ digital holography. Mar. Ecol. Prog. Ser. **473**: 29–51. doi:10.3354/meps10049

Teixeira. 1973. C. Preliminary studies of primary production in Ubatuba region (Lat. 23°30′S–Long. 45°06′W). Bol. Inst. Oceanogr. **22**: 49–58. doi:10.1590/S0373-55241973000100003

Thomson, R. E., and W. J. Emery. 2014. Data analysis methods in physical oceanography. Newnes.

Turner, J. T. 2004. The importance of small planktonic copepods and their roles in pelagic marine food webs. Zool. Stud. **43**: 255–266.

Urban-Rich, J., D. Fernández, and J. L. Acuña. 2006. Grazing impact on chromophoric dissolved organic matter (CDOM) by the larvacean *Oikopleura dioica*. Mar. Ecol. Prog. Ser. **317**: 101–110. doi:10.3354/meps317101

Villac, M. C., V. A. D. P. Cabral-Noronha, and T. D. O. Pinto. 2008. The phytoplankton biodiversity of the coast of the state of São Paulo, Brazil. Biota Neotrop. **8**: 152–173. doi:10.1590/S1676-06032008000300015

Welschmeyer, N. 1994. Fluorometric analysis of chlorophyll *a* in the presence of chlorophyll *b* and pheopigments. Limnol. Oceanogr. **39**: 1985–1992. doi:10.4319/lo.1994.39.8.1985

Yoshida, J., H. Nagashima, and W. J. Ma. 1987. A double diffusive lock-exchange flow with small density difference. Fluid Dyn. Res. **2**: 205–215. doi:10.1016/0169-5983(87)90030-X

Acknowledgments

We thank Hidekatsu Yamazaki for loaning the RINKO-profiler used in this study and for the advice on the appropriate sampling methodology. Mamoru Tanaka and Olga Sato for the helpful comments. Joseph Harari and Tiago Cortez for their assistance with the wind and sea level data. John Ryan for the help for creating Fig. 4. Leandro de la Cruz for the development of the image classification software and Matlab codes that helped us in processing image data. Technicians Mayza Pompeu and Mateus Chuqui for the analysis of nutrients. Maia Medeiros and Alessandra Gomes for for setting up the imaging system and providing technical support during its deployment. Marta Stephan, Eduarda Laurentino and Marcio Santana for assistance in the fieldwork. Kellie Terada for help with logistics for a J-1 student internship for S.B.P. during her time at the University of Hawai'i at Mānoa. The crew of the R/V *Veliger II*, from USP's Oceanographic Institute, for their valuable support in the fieldwork. The editor and the two anonymous reviewers for their suggestions and constructive comments. This study was funded in part by the Coordination for the Improvement of Higher Education Personnel—Brazil (CAPES)—Finance Code 001, and by a CNPq grant (310642/2017-5) to R.M.L.

Conflict of Interest

None declared.

Submitted 05 March 2020
Revised 22 July 2020
Accepted 19 September 2020

Associate editor: Kelly Benoit-Bird